J. Shanghai Jiao Tong Univ. (Sci.), 2024
https://doi.org/10.1007/s12204-024-2773-5

Design of a 6-DOF Master Robot for Robot-Assisted Minimally Invasive Surgery

CHENG Hongyu[1] (程泓宇), *ZHANG Han*[1] (张　涵), *WANG Shuang*[1,2] (王　爽), *XIE Le*[1,2*] (谢　叻)
(1. School of Materials Science and Engineering, Shanghai Jiao Tong University, Shanghai 200030, China;
2. Institute of Medical Robotics, Shanghai Jiao Tong University, Shanghai 200240, China)

Abstract: Master robots are integral components of teleoperated robot-assisted minimally invasive surgery systems. Among them, parallel mechanism-based 6-degree-of-freedom master robots are distinguished by low inertia and high-force feedback. However, complex kinematics and singularities are the main barriers limiting its usage. This study converts the Hexa-type 6-RUS mechanism into a master robot to construct master-slave teleoperation system. The clinical background is briefly introduced and a representative surgical robot is employed to analyze the master-slave mapping relationship. The inverse/forward kinematics, the Jacobian matrix, and the translation and orientation workspace are derived as the bases of master robot's application. The architecture parameters are optimized by the global transmission index to achieve better motion/force transmissibility. Based on the optimal result, the prototype and the master-slave control loop are constructed. Finally, the corresponding master-slave teleoperation experiment and model experiment demonstrate that the proposed master robot satisfies the basic need for medical application.
Keywords: master robot, master-slave teleoperation system, surgical slave robot, master-slave control
CLC number: TP242　　**Document code:** A

0 Introduction

As society ages, the demand for surgical interventions has been increasing steadily over the years. To address such significant demand, robot-assisted minimally invasive surgery (RMIS) has emerged as an efficient solution, providing the benefits of shorter operating time, smaller incisions, less bleeding, less pain, and faster recovery. As illustrated in Fig. 1, in a standard RMIS procedure, the surgeon controls the master robot to issue commands to the slave robot (surgical manipulator) and maneuver its movements while receiving visual and touch feedback[1]. In medical field, the slave robots always consist of multiple joints and are equipped with multiple surgical instruments, therefore containing multiple degrees-of-freedom (DOFs). Commonly, with multi-DOF slave device, the intuitive control requires the master device equipped with more DOFs. In our practice[2], commercialized 3 DOFs master robot Falcon presents limits in complex RMIS, while 6-DOFs master robots are better suited for the surgical slave robots with multi-instrument operations and multi-DOF motion. Therefore, there is an urge need to design a 6 DOFs master robot to accommodate with the multi-DOF requirement of medical slave robot.

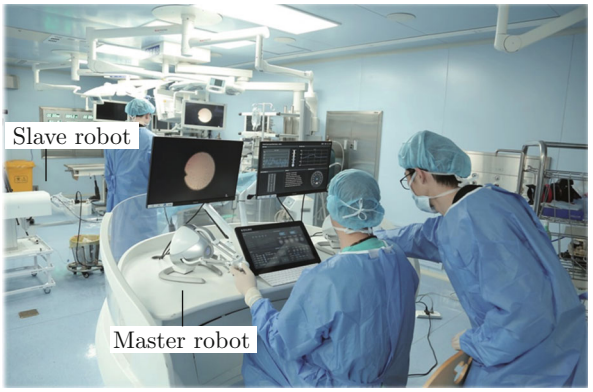

Fig. 1　Scheme of the robot-assisted minimally invasive surgery.

In recent years, various 6-DOF master robots have been proposed to facilitate remote-control operations, which can be broadly classified into three categories of mechanisms[3]: serial, parallel, and hybrid.

Received: 2023-12-19　**Accepted:** 2024-01-25
Foundation item: the National Natural Science Foundation of China (No. 62211540723), the Interdisciplinary Program of Shanghai Jiao Tong University (Nos. YG2023ZD05 and YG2023ZD14), the Quanzhou High-Level Talent Innovation and Entrepreneurship Project (No. 2021C003R), and the Research Project of Institute of Medical Robotics of Shanghai Jiao Tong University
*E-mail: lexie@sjtu.edu.cn

Compared with serial and hybrid ones, parallel manipulators (PMs) gain significant attention due to their high precision, fast response, and low inertia. Furthermore, the master handle fixed in the moving platform is more in line with human operating habits. Several investigations around parallel mechanism-based 6-DOF master devices have been proposed. Abeywardena and Chen[4] implemented a three-legged 6-DOF PM (i.e., MEPaM) as a master robot, whose leg is actuated by a 2-DOF planetary-system, and the motion/force is then transferred into the moving platform by several single DOF joints. Vulliez et al.[5] designed a novel 6-DOF master robot by combining two delta robots. The inner one connecting with the master handle provides 3-DOF translation, and the outer one enables the handle of a 3-DOF rotation by assembling a ball-screw joint. Jin et al.[6] enhanced a complete 6-DOF parallel mechanism with grasping capacity by adding two opposite prismatic joints and decoupling the grasping from the yaw motion by employing three auxiliary parallelograms, resulting in a 7-DOF master robot with all actuators fixed to the ground. However, the structures mentioned above take up relatively large volumes and are not adaptable for RMIS. Hence, there is an urge need to develop a compact, lightweight, and ergonomic master robot suitable for surgical interventions.

Among 6-DOF PMs, the 6-RUS Hexa-type PM has gained popularity in industries[7] with its high flexibility and light mobile platform. Six-RUS Hexa-type PM is a direct extension of the delta robot. However, the complexity of forward kinematics and the occurrence of singularities cast a shadow over its application. Yang et al.[8] have proposed different approaches to address this issue. Kühne et al.[9] added two extra RUS links to classical the 6-RUS Hexa-type PM, creating a novel redundantly-actuated octopod-type mechanism and defining quantitative criteria to optimize its performance. Lambert and Herder[10] adopted an optimization method based on the condition number of the Jacobian matrix called local conditioning index (LCI), which is commonly used in serial robots to avoid singularities. However, the redundantly actuated limbs increase the structural complexity and restrict the workspace. At the same time, the LCI index varies according to the coordinate frame and has limitations when applied to PMs[11]. In addition, the proposed master robots are lack of master-slave teleoperation experiments combined with actual slave surgical robot.

Accordingly, this paper presents a 6-RUS Hexa-type master robot for RMIS. The clinical background and the representative slave surgical robot are introduced. The Jacobian matrix and inverse/forward kinematics of the master robot are derived effectively, and the translation and orientation workspace are determined by integrating the geometric and numerical methods as the basis of master robot usage. Based on the global transmission index (GTI), the dimension synthesis is carried out for better motion/force transmissibility. The prototype is constructed based on the optimized result and the master-slave control system is constructed. The effectiveness of the proposed system is validated through corresponding master-slave teleoperation experiment and model experiment.

1 Description of Architecture and Kinematics

1.1 Clinical Background

Natural orifice transluminal endoscopic surgery (NOTES) is an innovation technology to perform surgery through natural body orifices. However, with limited surgical space and field of view, the direct operation of instruments requires great medical skill and may increase the risk of danger. Therefore, the master-slave teleoperation systems are widely adopted for NOTES which commonly employ a surgical robot as the slave part to enhance surgical flexibility while adopting a master robot to remotely control the motion of the surgical robot as well as receiving force feedback.

As illustrated in Fig. 2, a continuum surgical robot proposed in our previous work[12] designed specifically for transoral robotic surgery is utilized as the representative surgical robot. The slave robot system contains 4 controllable DOFs including deflection along the x and y axes, rotation around z axis and the translation of bio forceps inserted in the instrument channel, and its effectiveness has been proven through animal experiment[12]. However, the movement of such

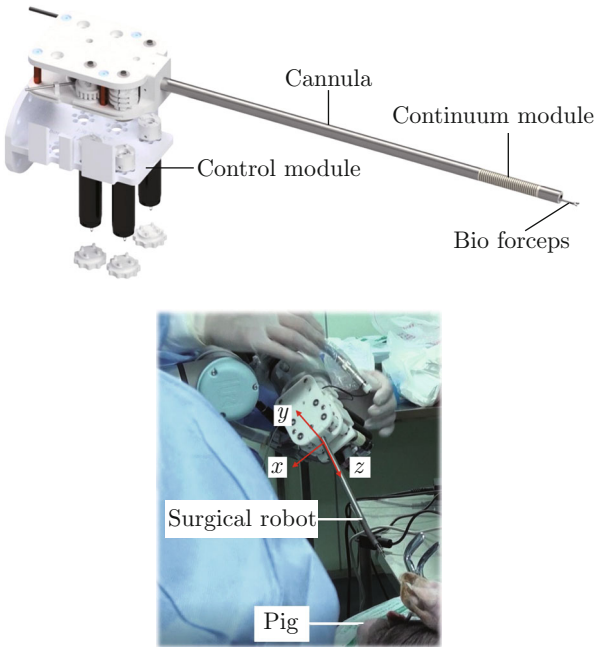

Fig. 2 Representative surgical robot for transoral surgery.

a slave surgical robot is relatively small and quite different from human's operation habit. In addition, it is difficult for the operator to observe the relative position of the robot in the surgical area. Therefore, a common solution is to construct a master-slave isomeric master robot, which is in line with human's operation habit and map the motion of master robot into the motion of slave robot in certain scale. Here, in Fig. 3, the master-slave mapping relationship is conducted based on the drive space, which is more intuitive during operation. The three coordinate axes of the slave robot are denoted by x_{s}, y_{s} and z_{s} while those of the master robot are noted by x_{m}, y_{m} and z_{m}. The master-slave mapping maps the movement of slave robot $(R_x^{\mathrm{s}}, R_y^{\mathrm{s}}, R_z^{\mathrm{s}}, T_z^{\mathrm{s}})$ into the movement of the master robot $(T_x^{\mathrm{m}}, T_y^{\mathrm{m}}, R_z^{\mathrm{m}}, T_z^{\mathrm{m}})$ respectively. The rest of this article is to discuss how to design a master robot with sufficient DOFs to control the movement the slave robot.

As explained in Ref. [8], to effectively perform the master-slave control, the master robot should meet the basic requirement proposed below. The workspace should be free of singularities, having a minimum volume of 100 mm × 100 mm × 100 mm and providing ±30° of rotational DOFs around all axes, which allows natural reaching motions including arm transport.

1.2 Mechanism Description

The kinematic arrangement of the 6-RUS Hexa-type PM is depicted in Fig. 4(a), the proposed CAD model is depicted in Fig. 4(b), and the moving platform is linked to the fixed base through six identical RUS limbs. Each RUS limb attaches to the fixed base by rotation joint $(A_i,\ i = 1, 2, \cdots, 6)$ with a radius R_1. Two adjacent rotation joints $(A_1\&A_2,\ A_3\&A_4,\ A_5\&A_6)$ are parallel to each other and perpendicular to the bisector of

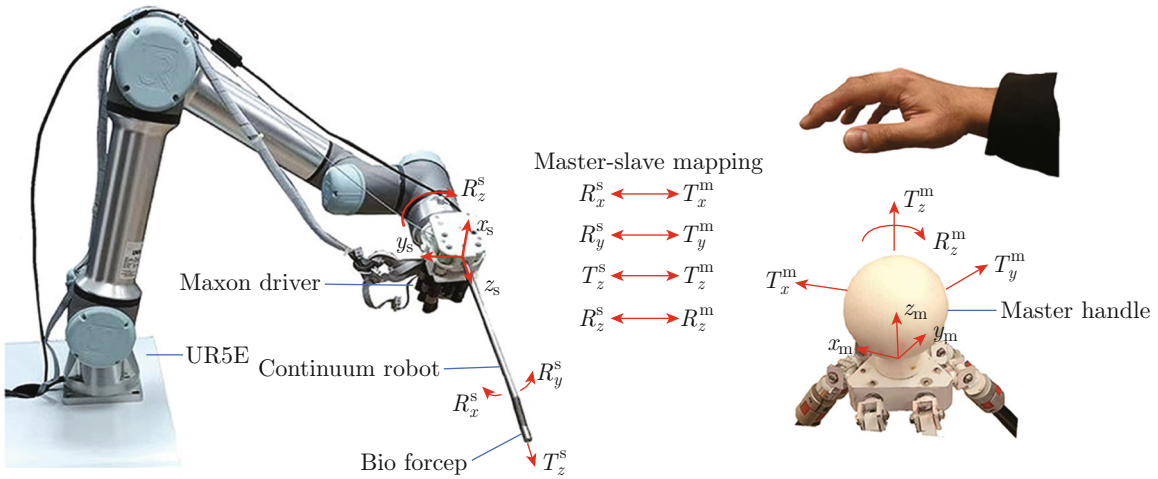

Fig. 3 Master-slave mapping relationship.

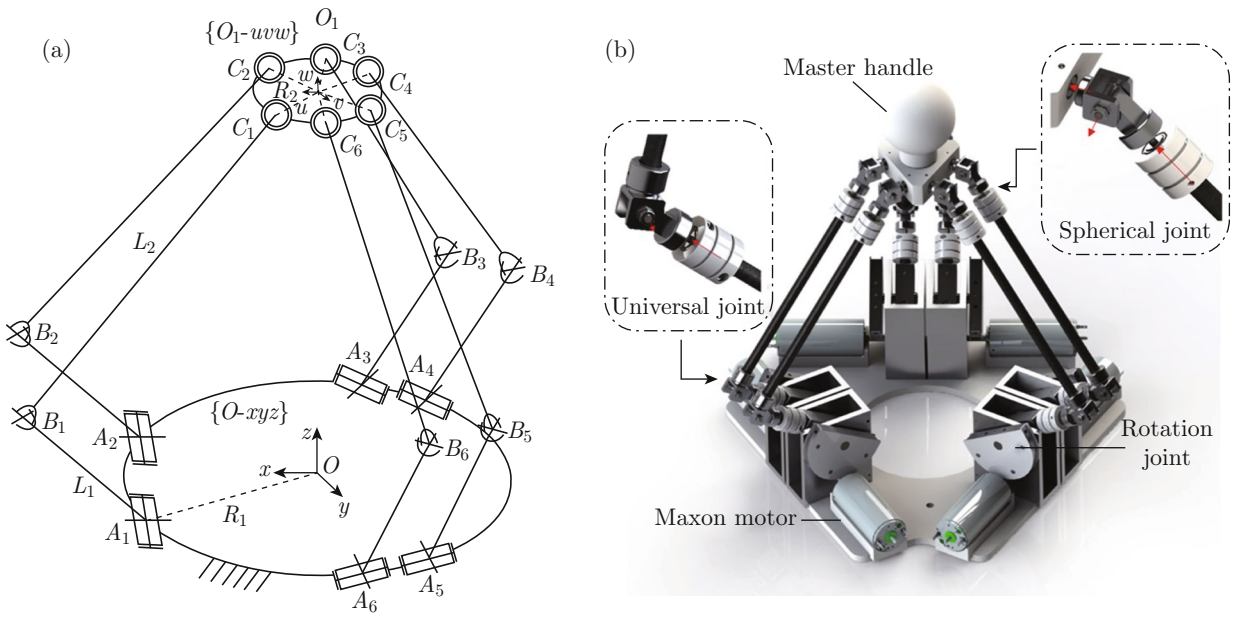

Fig. 4 Scheme of the Hexa-type 6-RUS PM. (a) Kinematic scheme; (b) CAD model.

$\angle A_iOA_j$, $i = 1, 3, 5$, $j = 2, 4, 6$. Six spherical joints (C_i, $i = 1, 2, \cdots, 6$) are evenly placed in the moving platform with a radius R_2. Each rotation joint and spherical joint are connected to a universal joint (B_i) by limb $\overrightarrow{A_iB_i}$ with length L_1 and limb $\overrightarrow{B_iC_i}$ with length L_2 respectively.

Before conducting a comprehensive kinematic analysis, two coordinate systems have to be established: the fixed base O-xyz and the moving platform O_1-uvw. The x axis runs along the mid-line between $\overrightarrow{OA_1}$ and $\overrightarrow{OA_2}$, the z axis is perpendicularly pointing up from the base, and the y axis is determined using the right-hand rule. Similarly, in O_1-uvw. The u axis runs along the mid-line between $\overrightarrow{OB_1}$ and $\overrightarrow{OB_2}$, the w axis is perpendicularly pointing up from the moving platform, and the v axis can be determined accordingly. To aid in the explanation that follows, the geometric parameters are defined as follows:

$$\left.\begin{aligned} \overrightarrow{OA_i} &= \Big(R_3\cos\Big(-\frac{\pi}{2}+i\frac{\pi}{3}\Big), \\ &\qquad R_2\sin\Big(-\frac{\pi}{2}+i\frac{\pi}{3}\Big), 0\Big)^{\mathrm{T}} \\ {}^{O_1}\overrightarrow{O_1C_i} &= \Big(R_2\cos\Big(-\frac{\pi}{2}+i\frac{\pi}{3}\Big), \\ &\qquad R_2\sin\Big(-\frac{\pi}{2}+i\frac{\pi}{3}\Big), 0\Big)^{\mathrm{T}} \\ i &= 1, 2, \cdots, 6 \end{aligned}\right\}, \tag{1}$$

where $R_3 = \sqrt{R_1^2 - R_2\sin\Big(\frac{\pi}{6}\Big)^2}$. Subsequent discussions are conducted in the fixed frame by default.

Moreover, some basic vectors should be preliminary defined. For a more intuitive and concise visualization, the position of the moving platform is typically represented by a vector $\boldsymbol{P}$ that extends from the base center O to the moving platform center by O_1, and the orientation is represented by rotation matrix ${}^{O}\boldsymbol{R}_{O_1}$ in Euler angle form.

1.3 Inverse Kinematics

The inverse kinematics of the 6-RUS PM yields analytical solutions for the actuated parameters $\boldsymbol{\Theta} = (\theta_1, \theta_2, \cdots, \theta_6)^{\mathrm{T}}$ when the moving platform's posture (position vector $\boldsymbol{P}$ and rotation matrix ${}^{O}\boldsymbol{R}_{O_1}$) is fixed. The main idea of inverse kinematics is to establish the close-loop equation. As illustrated in Fig. 5, by taking the limb i as an example, the position vector $\boldsymbol{P}$ can be expressed by

$$\boldsymbol{P} = \overrightarrow{OA_i} + \overrightarrow{A_iB_i} + \overrightarrow{B_iC_i} + {}^{O}\boldsymbol{R}_{O_1}\,{}^{O_1}\overrightarrow{C_iO_1}. \tag{2}$$

Notice that in $\Delta A_iB_iC_i$, the values of $\|\overrightarrow{A_iC_i}\|$, $\|\overrightarrow{A_iB_i}\|$ and $\|\overrightarrow{B_iC_i}\|$ can be easily achieved, where $\overrightarrow{A_iC_i} = -\overrightarrow{OA_i} + \boldsymbol{P} + {}^{O}\boldsymbol{R}_{O_1}\,{}^{O_1}\overrightarrow{C_iO_1}$. While in the local coordinate system A_i-$x_iy_iz_i$, $\overrightarrow{A_iB_i}$ can be expressed as a function of joint variable θ_i, which is expressed by

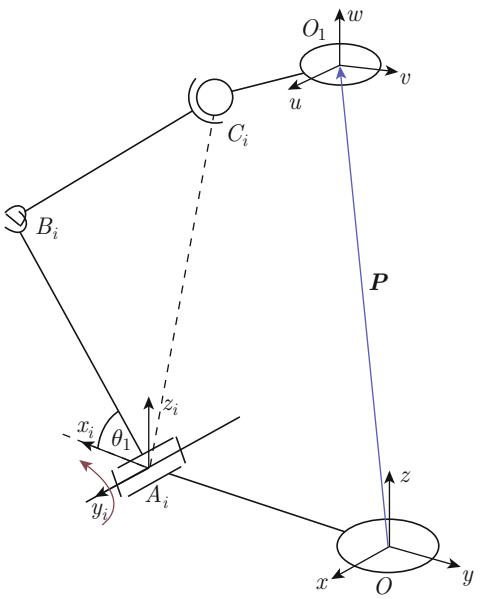

Fig. 5 Kinematic scheme of Hexa-type 6-RUS PM limb.

$\overrightarrow{A_iB_i} = L_1\cos\theta_i\boldsymbol{X}_i + L_2\sin\theta_i\boldsymbol{Z}_i$, where $\boldsymbol{X}_i$ is pointing along x_i and $\boldsymbol{Z}_i$ is pointing z_i. Thus, the constrain equation can be given by

$$\|\overrightarrow{B_iC_i}\| = \|\overrightarrow{A_iB_i} - \overrightarrow{A_iC_i}\| = L_2. \tag{3}$$

By adopting Weierstrass substitution, the analytical solutions can be expressed by

$$\beta_i = 2\arctan\Big(\frac{-b_i \pm \sqrt{b_i^2 - 4a_ic_i}}{2a_i}\Big), \quad i = 1, 2, \cdots, 6. \tag{4}$$

And

$$\begin{aligned} a_i &= m_i - 2L_1\overrightarrow{A_iC_i}\cdot\boldsymbol{X}_i, \\ b_i &= 4L_1\overrightarrow{A_iC_i}\cdot\boldsymbol{Z}_i, \\ c_i &= 2L_1\overrightarrow{A_iC_i}\cdot\boldsymbol{X}_i + m_i, \\ m_i &= L_2^2 - L_1^2 - \|\overrightarrow{A_iC_i}\|^2. \end{aligned}$$

It should be noted that the analytic solution exists 2^6 potential combinations of actuated angles for a given posture. Still, only the angles consistent with Fig. 4 are permissible.

1.4 Jacobi Matrix

The Jacobi Matrix can be achieved by taking the derivative of the closed loop equation with respect to time, and the result is given by

$$\boldsymbol{V}_{O_1} = \boldsymbol{\omega}_{A_i}\times\overrightarrow{A_iB_i} + \boldsymbol{\omega}_{B_i}\times\overrightarrow{B_iC_i} - \boldsymbol{\omega}_{O_1}\times\overrightarrow{O_1C_i}, \tag{5}$$

where $\boldsymbol{V}_{O_1}$ and $\boldsymbol{\omega}_{O_1}$ represent the linear velocity and angular velocity of the moving platform respectively, $\boldsymbol{\omega}_{A_i}$

represents the angular velocity of the actuated joints while $\boldsymbol{\omega}_{B_i}$ is unknown and must be eliminated through mathematical method. By dot multiplying $\overrightarrow{B_iC_i}$ on both sides of the equation and using the property of reciprocal product, the equation can be rearranged by

$$\overrightarrow{B_iC_i}\cdot\boldsymbol{V}_{O_1}+({}^{O}\boldsymbol{R}_{O_1}{}^{O_1}\overrightarrow{O_1C_i}\times\overrightarrow{B_iC_i})\cdot\boldsymbol{\omega}_{O_1}= (\overrightarrow{A_iB_i}\times\overrightarrow{B_iC_i})\cdot\boldsymbol{\omega}_{A_i}, \tag{6}$$

which tells the speed relationship between the actuated joints and the moving platform. The simplified and general form can be written as

$$\boldsymbol{J_x}\dot{\boldsymbol{x}}=\boldsymbol{J_q}\dot{\boldsymbol{q}}, \tag{7}$$

where $\dot{\boldsymbol{x}}$ and $\dot{\boldsymbol{q}}$ are the velocities of master robot handle and joints respectively, and $\boldsymbol{J}=\boldsymbol{J_x}^{-1}\boldsymbol{J_q}$ is the Jacobi matrix of the master robot.

Jacobi matrix is not only the medium between the velocity of actuated joints and the velocity of the moving platform, but also the bridge between the torque of the actuated joints and the force applied in the moving platform. This relationship can be deduced by the virtual work principle[13] and given by

$$\boldsymbol{F}=\boldsymbol{J}^{\mathrm{T}}\boldsymbol{\tau}, \tag{8}$$

where $\boldsymbol{F}$ is the force applied at the center point of the moving platform, and $\boldsymbol{\tau}$ represents the torque generated by each actuated joint. When the master robot is moved to a certain position, the torque required to provide force feedback can be calculated by the formula and realize real-time force feedback.

1.5 Forward Kinematics

The forward kinematics determines the posture of the moving platform with given actuated joints. Due to the highly nonlinear nature of the forward kinematics equation, few analytical solutions of 6-DOF parallel structures can be obtained, and in most cases[13], numerical methods are adopted to solve the forward kinematics in an iterative form. Notice that a feasible way to describe the relationship between the actuated angles and the posture is provided in Eq. (3). The forward kinematics can be transferred into a nonlinear equation by

$$\boldsymbol{G}(\boldsymbol{Y})=(g_1(\boldsymbol{Y}),g_2(\boldsymbol{Y}),\cdots,g_6(\boldsymbol{Y}))^{\mathrm{T}}= \boldsymbol{G}(\boldsymbol{Y}_0)+\boldsymbol{J}\mathrm{d}\boldsymbol{q}=\boldsymbol{0}, \tag{9}$$

where $g_i=L_2-\left\|\overrightarrow{A_iC_i}-\overrightarrow{A_iB_i}\right\|$, and $\boldsymbol{q}$ is the simultaneous position of motor joints.

The proposed nonlinear equations can be solved efficiently using the trust-region method with a given initial posture $\boldsymbol{Y}_0$ and a real-time updated Jacobian matrix $\boldsymbol{J}$. In practice, the position of the master robot needs to be calibrated into the center beforehand. Then the forward kinematics can simultaneously track the trajectory of the master handle movement by reading the pulse number of encoders assembled in the actuated joints.

2 Workspace Determination

For the 6-DOF parallel mechanism, it becomes impossible to graphically illustrate the workspace with decoupled DOFs. Therefore, a practical approach is to partition the workspace into two distinct 3D subspaces: the translation workspace and the orientation workspace, and then identify the individual boundaries of each subspace, providing a more precise visualization of the overall workspace.

2.1 Definition of Constraints

Before determining the workspace, an essential step is establishing several fundamental constraints[14] that restrict the motion of the moving platform. These constraints include kinematic constraints and structural constraints. The kinematics constraints can be determined through inverse kinematics in Eq. (4), which is given by

$$b_i^2-4a_ic_i\geqslant 0,\quad i=1,2,\cdots,6. \tag{10}$$

In fact, the region that these inequalities surround is the maximum range in which a 6-RUS mechanism can move without considering the structural constraints. However, the region is also limited by the structural constraints. The structural constraints refer to the mechanical limits of both the actuated joints and passive joints as well as the link interface. Actuated joints are intentionally limited to $[0,\pi/2]$, while the range of the passive joints depends on their specific structural characteristics. For the universal joint C_i, the maximum angle between $\overrightarrow{A_iB_i}$ and $\overrightarrow{B_iC_i}$ is defined as ϕ_{B_i}, while for the spherical joint B_i, the maximum angle between $\overrightarrow{B_iC_i}$ and the moving platform is ϕ_{C_i}, so the constraint equations can be written as

$$\left.\begin{aligned}&\frac{\overrightarrow{A_iB_i}\cdot\overrightarrow{B_iC_i}}{\left|\overrightarrow{A_iB_i}\right|\left|\overrightarrow{B_iC_i}\right|}\leqslant\cos\phi_{B_i}\\&\frac{\overrightarrow{C_iB_i}\cdot(-{}^{O}\boldsymbol{R}_{O_1}{}^{O_1}\overrightarrow{O_1C_i})}{\left|\overrightarrow{C_iB_i}\right|\left|-{}^{O}\boldsymbol{R}_{O_1}{}^{O_1}\overrightarrow{O_1C_i}\right|}\leqslant\cos\phi_{C_i}\end{aligned}\right\}. \tag{11}$$

In Hexa-type 6-RUS PM, the link interface always exists between two passive limbs. Assuming that the limbs in the master device can be approximated as cylinders with a diameter d_{c}, the link interface restriction can be expressed by a distance function:

$$d(\overrightarrow{A_iB_i},\overrightarrow{A_jB_j})\geqslant d_{\mathrm{c}},\quad i,j=1,2,\cdots,6,\quad j\neq i. \tag{12}$$

2.2 Translation Workspace

The translation workspace of PM is defined as all possible locations of the moving platform center that can be reached with a given orientation. In current structure, there is no singular point inside the translation

workspace, so the boundary points of the workspace can be determined by the traversal search method. However, common traversal method[8] requires a large amount of computation in determining the workspace but also with limited result. Therefore, in order to efficiently determine the boundary points/curve and adopt it in the optimizing of structural parameters, the following solution algorithm is proposed.

Algorithm 1: Translation workspace determination
Input: The structural parameters R_1, R_2, L_1, L_2, the constraint function $\boldsymbol{G}$, rotation matrix ${}^{O}\boldsymbol{R}_{O_1}$
Output: The boundary points of the translation workspace.
1: Determine the boundary $z_{\min}$ and $z_{\max}$ along z axis.
2: **for** $z_i = z_{\min} - 1$ to $z_{\max}$ **do**
3: **for** $\alpha = 0$ to 2π **do**
4: $\rho = 0$
5: **while** true **do**
6: **If** $\boldsymbol{G}({}^{O}\boldsymbol{R}_{O_1}, \rho\cos\alpha, \rho\sin\alpha, z_i)$ **then**
7: $\rho = \rho + \Delta\rho$
8: **else if** $\rho - \Delta\rho > 0$ **then**
9: Store $(\rho\cos\alpha, \rho\sin\alpha, z_i)$
10: **end if**
11: **break**
12: **end if**
13: **end while**
14: **end for**
15: **end for**
16: **return** $(\rho\cos\alpha, \rho\sin\alpha, z_i)$

Compared with other algorithms[15], this algorithm has the advantage of its ability to approximate the values of workspace boundaries with a relatively fast computational speed, which is vital for the subsequent structural optimization.

2.3 Orientation Workspace

The orientation workspace is defined as the set of all possible orientations that can be reached while maintaining the position of the moving platform center O_1. A numerical method similar to the determination of translation workspace is adopted to generate the complete orientation workspace. However, in order to better illustrate the orientation angles, the Tile & Torsion angle representation ${}^{O}\boldsymbol{R}_{O_1}(\phi, \theta, \sigma)$ is employed, which can avoid the description singularity[14] in Euler angle, and widely adopted in parallel robots. Then, the similar algorithm is presented as follows:

Algorithm 2: Orientation workspace determination
Input: The structural parameters R_1, R_2, L_1, L_2, the constraint function $\boldsymbol{G}$, position $\boldsymbol{P}$.
Output: The boundary points of the translation workspace.
1: Determine the boundary $\sigma_{\min}$ and $\sigma_{\max}$.
2: **for** $\sigma_i = \sigma_{\min}$ to $\sigma_{\max}$ **do**
3: **for** $\theta = 0$ to π **do**
4: $\phi = 0$
5: **while** true **do**
6: **If** $\boldsymbol{G}(P, \phi, \theta, \sigma_i)$ **then**
7: $\phi = \phi + \Delta\phi$
8: **else if** $\phi - \Delta\phi > 0$ **then**
9: Store (ϕ, θ, σ_i)
10: **end if**
11: **break**
12: **end if**
13: **end while**
14: **end for**
15: **end for**
16: **return** (ϕ, θ, σ_i)

3 Optimal Design

In addition, the singularity of this mechanism can occur when the moving platform is coplanar with two terminal RUS limbs as well as the passive limb and the actuated limb close to collinear. Therefore, the following discussion aims to avoid singularity, meet this design criteria and obtain better motion/force transmissibility.

3.1 Index Definition

Kinematic performance analysis is a key issue for the design of PMs and can identify the singularity based on motion/force transmission indices proposed in Ref. [16]. Before calculating the indices, the screw modeling of the RUS limb needs to be firstly constructed. The input twist screw (ITS) $\boldsymbol{S}_{I_i}$ of limb i is defined as the rotation motion of actuated joints, while the transmission wrench screw (TWS) $\boldsymbol{S}_{T_i}$ of limb i is reciprocal to all input twist screws $\boldsymbol{S}_{I_j}$, $j \neq i$ of RUS limb except $\boldsymbol{S}_{I_i}$, which can be derived by undetermined coefficient method. The result indicates that the $\boldsymbol{S}_{T_i}$ is a pure force along $\overrightarrow{B_iC_i}$. The output twist screw (OTS) $\boldsymbol{S}_{O_i}$ which represents the instantaneous movement induced by $\boldsymbol{S}_{T_i}$ can be derived by constructing the augmented matrix[17]. Then, the local transmission index (LTI) defined by energy coefficient[10] can be determined by

$$\left.\begin{aligned} \lambda_i &= \frac{|\boldsymbol{S}_{T_i} \circ \boldsymbol{S}_{I_i}|}{|\boldsymbol{S}_{T_i} \circ \boldsymbol{S}_{I_i}|_{\max}} \\ \eta_i &= \frac{|\boldsymbol{S}_{T_i} \circ \boldsymbol{S}_{O_i}|}{|\boldsymbol{S}_{T_i} \circ \boldsymbol{S}_{O_i}|_{\max}} \\ \kappa &= \min\{\lambda_i, \eta_i\} \\ i &= 1, 2, \cdots, 6 \end{aligned}\right\}, \tag{13}$$

where λ_i denotes the input transmission index (ITI) of limb i, and η_i denotes the output transmission index (OTI) of limb i. In addition, κ (LTI) ranges in $[0, 1]$ is a frame-free index, and a larger κ indicates better motion/force transmissibility and a larger distance from

reaching singularity configuration. For the common application, $\kappa \geqslant 0.3$ can prevent the PMs from reaching singular configurations[18].

3.2 Parameter Design Space

Dimension synthesis requires the abstraction of optimized parameters from the mechanical structure and a reduction in their dimensions. In the optimization design, there are four parameters to be optimized: R_1, R_2, L_1, L_2 while the proportion between the moving platform and the static platforms is pre-limited to $R_1 = \lambda R_2$. According to engineering design experience[19], λ is pre-set in 1.8. Therefore, the parameters left to be optimized are R_1, L_1, L_2 and they are normalized by

$$D = \frac{R_1 + L_1 + L_2}{3}, \tag{14}$$

where D is a non-dimensional factor, while $r_1 = R_1/D$, $l_1 = L_1/D$, $l_2 = L_2/D$ are three non-dimensional parameters.

In addition, the length of the limbs is restricted by $0 < r_1, l_1, l_2 < 3$, $l_1 < l_2$ and the design space is constructed in Fig. 6(a), delimited by dotted lines. For better visualization, the region is projected onto a planar view through projection transformation $s = r_1$, $t = (l_2 - l_1)/\sqrt{3}$, as shown in Fig. 6(b).

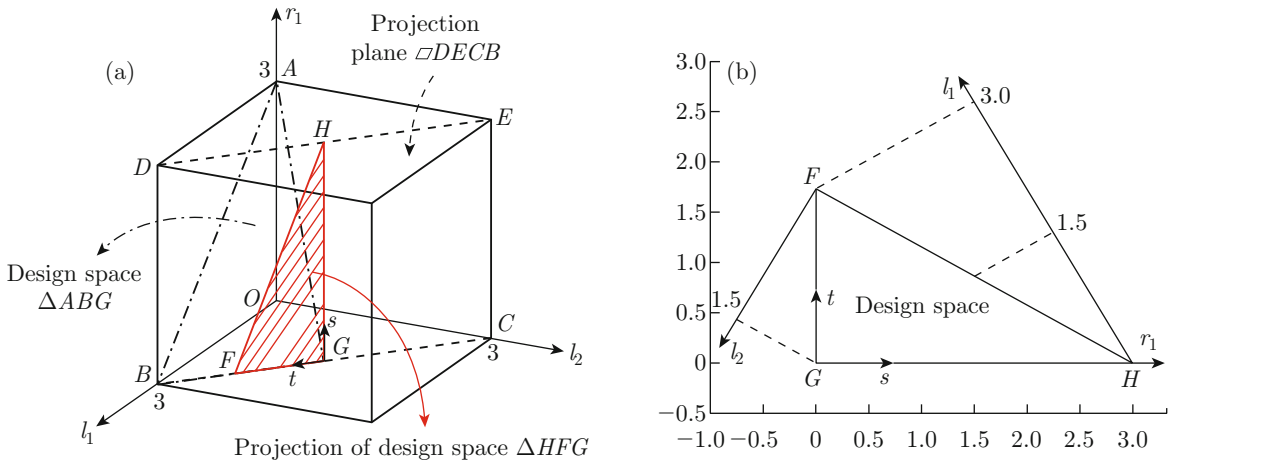

Fig. 6 Parameter design space: (a) 3D view; (b) Planar view.

3.3 Dimension Synthesis

Due to the multi-DOFs in the 6-RUS mechanism, optimizing within its workspace involves discretizing the 6-dimensional parameters, resulting in high computational complexity and time-consuming calculations. Moreover, the design requirements for the master robot do not necessitate the mechanism to achieve a globally optimal solution. Therefore, under the design criterion, the parameters are optimized within the translation workspace under the Euler angle sets: (0°, 0°, 0°), (30°, 0°, 0°), (0°, 30°, 0°), and (0°, 0°, 30°). To evaluate the performance of the master robot within the workspace, two metrics are defined, namely:

$$\gamma_{\mathrm{GTI}} = \frac{\int_{\mathrm{GW}} \kappa \mathrm{d}W}{\int_{\mathrm{GW}} \mathrm{d}W}, \tag{15}$$

where, W represents translation workspace; GW is the high-quality translation workspace, among which all set of points' $\kappa > 0.3$, and γ_{GTI} qualifies the performance of the master robot's movement within the GW. Therefore, the optimization equation for the master robot's parameters can be written as

$$\left.\begin{array}{l} \text{find} \quad \boldsymbol{X} = (r_1, l_1, l_2)^{\mathrm{T}} \\ \max \quad \gamma_{\mathrm{GTI}}(\boldsymbol{X}) \end{array}\right\}, \tag{16}$$
$$\text{s.t.} \quad 0 < r_1, l_1, l_2 < 3; r_1 + l_1 + l_2 = 3, \quad l_1 < l_2.$$

According to this optimization equation, the performance atlas can be plotted in the parameter design space. However, as the boundary of the translation workspace is difficult to represent as a continuous function, Algorithm 1 is employed to determine the boundary points corresponding to each set of structural parameters. Then, discrete points are uniformly generated within the numerical boundaries, and the equation is then numerically solved.

The corresponding performance atlas is presented in Figs. 7(a)—7(d), while the optimal region, i.e., the common area, is presented in Fig. 7(e). In order to achieve a compact design, the parameters: $r_1 = 0.765$, $r_2 = 0.255$, $l_1 = 1.635$, $l_2 = 0.600$ are selected as a candidate ratio for the fabrication of the master device.

To ensure a relatively small volume of the entire device and be adapted to the selected motors, the normalization factor is selected as $D = 125$, and the

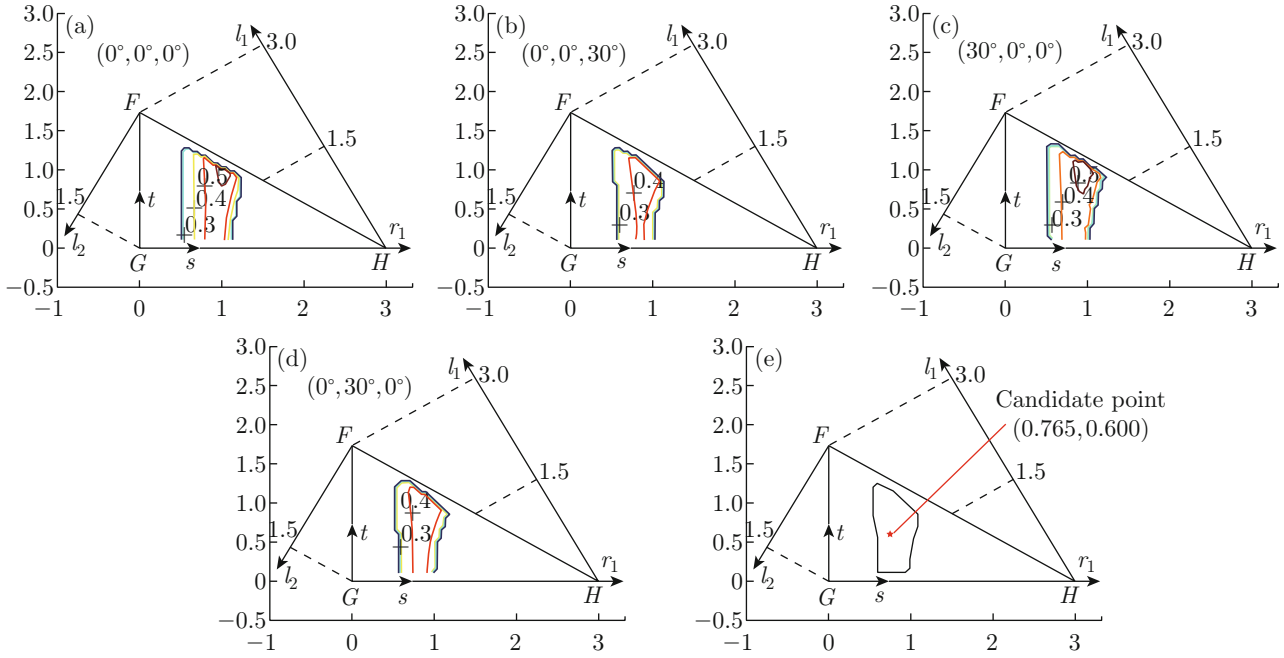

Fig. 7 Performance atlas. (a) (0°, 0°, 0°); (b) (0°, 0°, 30°); (c) (30°, 0°, 0°); (d) (0°, 30°, 0°); (e) Optimal area.

architecture parameters of the master device are eventually set to $R_1 \approx 96.0\,\text{mm}$, $R_2 \approx 32.0\,\text{mm}$, $L_1 \approx 75\,\text{mm}$, and $L_2 \approx 205\,\text{mm}$.

3.4 Prototype and Experiment

Based on the selected architecture parameters above, the master robot and the corresponding continuum robot are implemented in Fig. 8. The master robot is capable of translating to a maximum range of 120 mm × 120 mm × 110 mm while rotating to 45° around x and y axes and ±70° around z axis at maximum. The motion of the handle is magnified by the capstans with a transmission ratio of 6 and is detected by six DC motors (RE30, Maxon Motor AG, Switzerland) with optical encoders (HEDL 5540, Maxon Motor AG, Switzerland). The motion is then reconstructed by forward kinematics at a rate of 100 Hz.

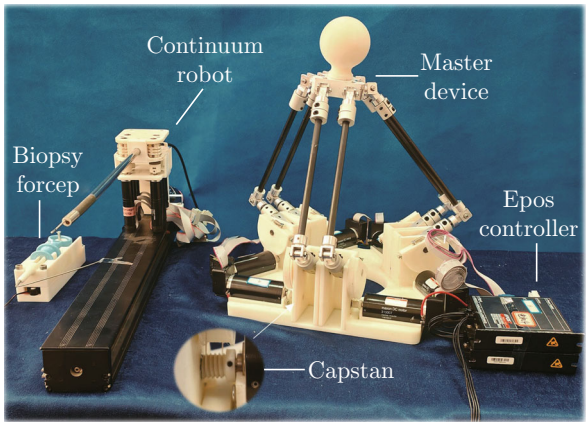

Fig. 8 Overall set of master-slave teleoperation system.

As shown in Fig. 9, the slave surgical robot and the master device in the master-slave teleoperation system are connected and exchange messages from a personal computer (PC) via control modules (EPOS2, Maxon Motor AG, Switzerland) through USB interfaces. Under the master-slave control loop, the surgeon controls the handle to control the master robot. The input motion $\boldsymbol{X}_\text{M}$ of the surgeon will be instantaneously read by motor encoders and reconstructed in PC. The PC will map the motion $\boldsymbol{X}_\text{M}$ on a small scale to the slave robot ($\boldsymbol{X}_\text{S}$) and the slave robot will be controlled to contact with patients. At the same time, the surgeon can receive visual feedback in real time through the microscope assembled in the surgical robot. During this control loop, the safety and stability of the whole system lie in high-speed teleoperation, master-slave motion scaling, and filtering method. To verify the performance of this system, an experiment is conducted in which the operator controls the movement of the continuum robot through the master handle. The result is illustrated in Fig. 10. The operation video is available via https://www.bilibili.com/video/BV1pj411A7Ws/.

In the current research, improved master robot and slave robot are constructed to perform the model experiment in transoral robotic surgery. As illustrated in Fig. 11, the result demonstrates that under the control of the master robot, the slave robot can reach the esophagus of the mannequin without making contact with the tissue in the cavity. In the future, this master robot will be applied to the control of different types of slave surgical robots[20-21].

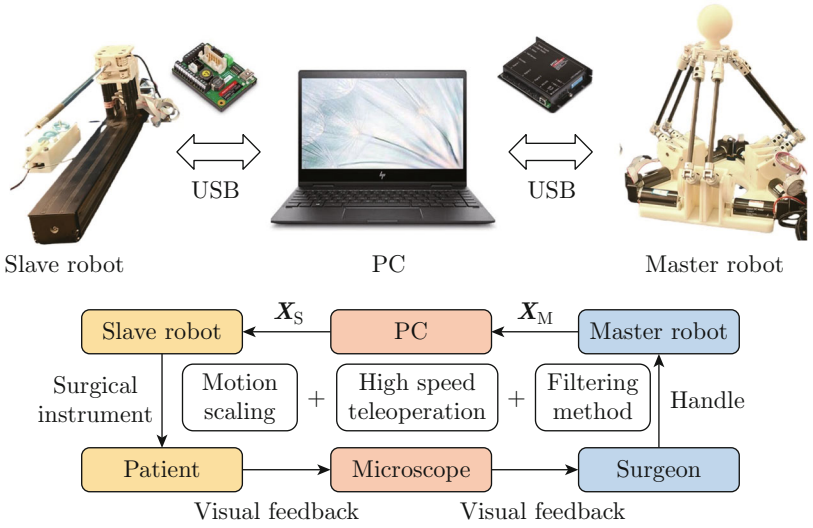

Fig. 9 Master-slave control loop of teleoperation system.

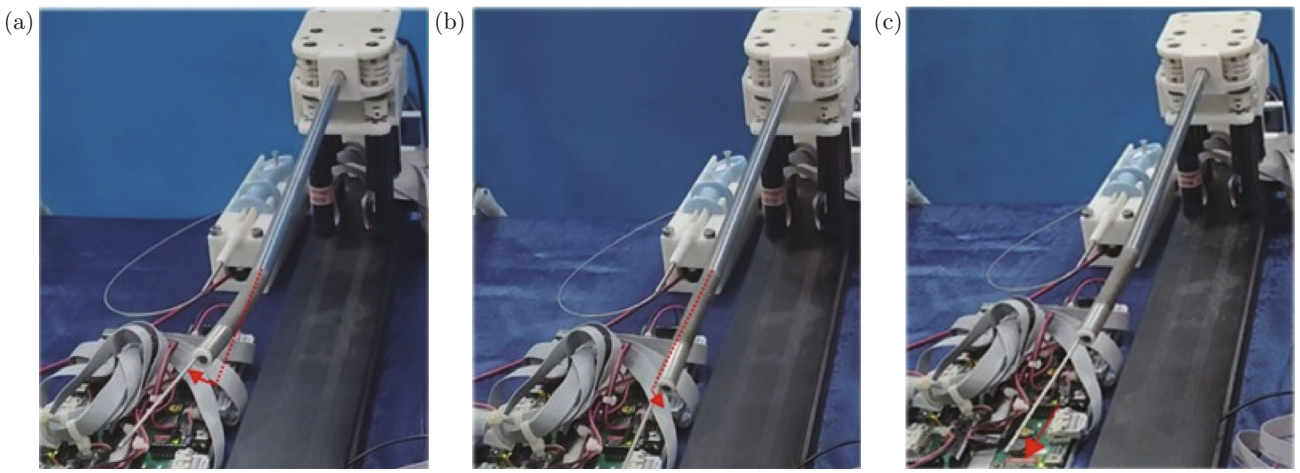

Fig. 10 Master-slave teleoperation experiment. (a) Deflexion along x axis; (b) Deflexion along y axis; (c) Translation along z axis.

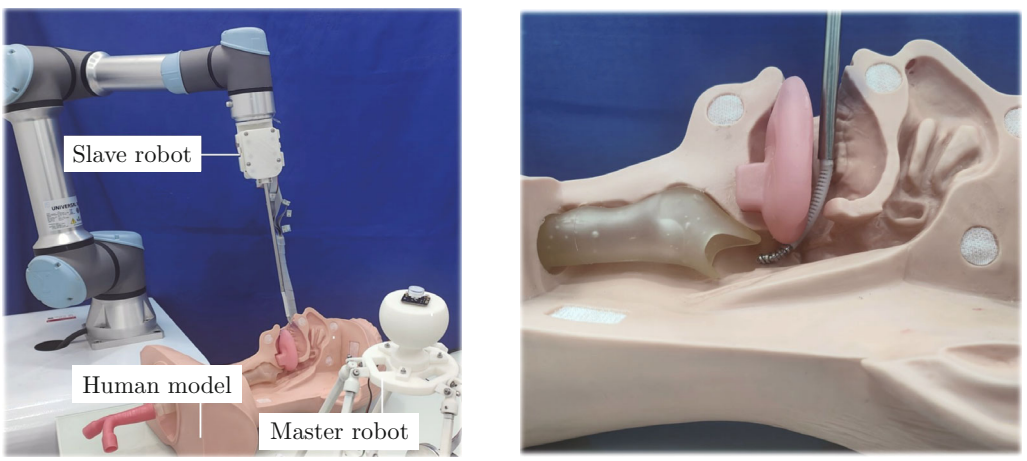

Fig. 11 Human model experiment.

4 Conclusion

This study presents the design of a Hexa-type 6-RUS master robot for minimally invasive surgery. The kinematics is derived and the workspace algorithm is proposed as the basis of the optimization procedure. Dimension synthesis is conducted to avoid singularity

and achieve better motion/force transmissibility. An optimized ratio with improved kinematics performance is obtained through the GTI and GWI indices. Finally, the prototype is fabricated, the master slave control loop is conducted, and the corresponding master-slave teleoperation experiment and model experiment are performed. The results demonstrate that the master robot can meet the basic requirements. A faster and more robust algorithm with force feedback control needs to be discussed in the future.

Conflict of Interest The authors declare that they have no conflict of interest.

References

[1] OMISORE O M, HAN S P, XIONG J, et al. A review on flexible robotic systems for minimally invasive surgery [J]. *IEEE Transactions on Systems, Man, and Cybernetics: Systems*, 2022, **52**(1): 631-644.

[2] WANG S, LIU Z, SHU X P, et al. Mechanism design and force sensing of a novel cardiovascular interventional surgery robot [J]. *The International Journal of Medical Robotics and Computer Assisted Surgery*, 2022, **18**(4): e2406.

[3] TORABI A, NAZARI A A, CONRAD-BALDWIN E, et al. Kinematic design of linkage-based haptic interfaces for medical applications: A review [J]. *Progress in Biomedical Engineering*, 2021, **3**(2): 022005.

[4] ABEYWARDENA S, CHEN C. Implementation and evaluation of a three-legged six-degrees-of-freedom parallel mechanism as an impedance-type haptic device [J]. *IEEE/ASME Transactions on Mechatronics*, 2017, **22**(3): 1412-1422.

[5] VULLIEZ M, ZEGHLOUL S, KHATIB O. Design strategy and issues of the Delthaptic, a new 6-DOF parallel haptic device [J]. *Mechanism and Machine Theory*, 2018, **128**: 395-411.

[6] JIN L X, DUAN X G, LI C S, et al. Design of a novel parallel mechanism for haptic device [J]. *Journal of Mechanisms and Robotics*, 2021, **13**(4): 045001.

[7] LALIBERTÉ T, ABDALLAH M, GOSSELIN C. A backdrivable 6-dof parallel robot for sensorless dynamically interactive tasks [J]. *Robotics and Computer-Integrated Manufacturing*, 2024, **86**: 102642.

[8] YANG Y, ZHANG Y R, ZHANG Y J, et al. Design and analysis of a new six-DOF parallel haptic device with singularity-free task workspace [C]//*ASME 2008 International Design Engineering Technical Conferences and Computers and Information in Engineering Conference*. Brooklyn: ASME, 2009: 1131-1139.

[9] KÜHNE M, POTZY J, GARCÍA-ROCHÍN R, et al. Design and evaluation of a haptic interface with octopod kinematics [J]. *IEEE/ASME Transactions on Mechatronics*, 2017, **22**(5): 2091-2101.

[10] LAMBERT P, HERDER J L. A 7-DOF redundantly actuated parallel haptic device combining 6-DOF manipulation and 1-DOF grasping [J]. *Mechanism and Machine Theory*, 2019, **134**: 349-364.

[11] WANG J S, WU C, LIU X J. Performance evaluation of parallel manipulators: Motion/force transmissibility and its index [J]. *Mechanism and Machine Theory*, 2010, **45**(10): 1462-1476.

[12] FENG F, ZHOU Y, HONG W Z, et al. Development and experiments of a continuum robotic system for transoral laryngeal surgery [J]. *International Journal of Computer Assisted Radiology and Surgery*, 2022, **17**(3): 497-505.

[13] TAGHIRAD H D. Parallel robots: Mechanics and control [M]. Boca Raton: CRC Press, 2013.

[14] BONEV I A, RYU J. A new approach to orientation workspace analysis of 6-DOF parallel manipulators [J]. *Mechanism and Machine Theory*, 2001, **36**(1): 15-28.

[15] CISNEROS-LIMÓN R, VÁZQUEZ-GONZÁLEZ J L, MENDOZA-VÁZQUEZ J R. Workspace analysis of a 6-RSS parallel robot considering non-ideal spherical joints [C]//*2015 IEEE/RSJ International Conference on Intelligent Robots and Systems*. Hamburg: IEEE, 2015: 3176-3181.

[16] LIU X J, WU C, WANG J S. A new approach for singularity analysis and closeness measurement to singularities of parallel manipulators [J]. *Journal of Mechanisms and Robotics*, 2012, **4**(4): 1.

[17] CHEN C, ANGELES J. Generalized transmission index and transmission quality for spatial linkages [J]. *Mechanism and Machine Theory*, 2007, **42**(9): 1225-1237.

[18] WANG L P, XU H Y, GUAN L W. Optimal design of a 3-PUU parallel mechanism with 2R1T DOFs [J]. *Mechanism and Machine Theory*, 2017, **114**: 190-203.

[19] MENG Q Z, LIU X J, XIE F G. Design and development of a Schönflies-motion parallel robot with articulated platforms and closed-loop passive limbs [J]. *Robotics and Computer-Integrated Manufacturing*, 2022, **77**: 102352.

[20] DAI Q L, XU M Q, SUN X D, et al. Eye robotic system for vitreoretinal surgery [J]. *Journal of Shanghai Jiao Tong University* (*Science*), 2022, **27**(1): 1-6.

[21] LI R, CHEN F, YU W W, et al. A novel cable-driven soft robot for surgery [J]. *Journal of Shanghai Jiao Tong University* (*Science*), 2024, **29**(1): 60-72.